DOI: http://dx.doi.org/10.1590/2179-10742017v16i2794

Experimental and numerical investigation of the microwave dielectric properties of the $MgTiO_3$ ceramic matrix added with $CaCu_3Ti_4O_{12}$

P.W.S. Oliveira[a,b,c], G.F.M. Pires Junior[a,b,d], A.J.M. Sales [a,b], H.O. Rodrigues[a,b,e] and A.S.B. Sombra[a,b]

[a]Departamento de Engenharia de Teleinformática-UFC, Caixa Postal 6007, CEP 60755-640, Fortaleza, Ceará, Brazil
[b]Laboratório de Telecomunicações e Ciência e Engenharia dos Materiais (LOCEM), Caixa Postal 6030, CEP 60455-760, Fortaleza, Ceará, Brazil.
[c]Instituto Federal de Educação, Ciência e Tecnologia do Ceará, Campus Fortaleza, CEP 60040-215, Fortaleza, Ceará, Brazil.
[d]Instituto Federal de Educação, Ciência e Tecnologia do Ceará, Campus Sobral, CEP 62042-030, Sobral, Ceará, Brazil.
[e]Instituto Federal de Educação, Ciência e Tecnologia do Ceará, Campus Quixadá, CEP 63400-00, Cedro, Ceará, Brazil.

***Abstract*— This paper describes an experimental and numerical investigation of the dielectric resonators based on the $MgTiO_3$ ceramic matrix, which relates to their dielectric properties in microwave. The resonators are compounds of the $MgTiO_3$ added with 4, 6, 8, 10 and 12 wt% of the $CaCu_3Ti_4O_{12}$. The manufacturing process of the resonators is based on the solid-state method. The properties of the permittivity and dielectric loss are elucidated using the Hakki and Coleman´s method. The experimental measurements of the dielectric resonators, acting as antennas, provide some results as return loss, gain, efficiency, bandwidth and input impedance. These results are coherent with the numerical investigation. The addition of the perovskite $CaCu_3Ti_4O_{12}$ in the $MgTiO_3$ ceramic matrix increased the value of the dielectric constant and it was obtained a higher value of 21.01 for the sample $MgTiO_3$ added with 12% $CaCu_3Ti_4O_{12}$. The temperature coefficient of resonant frequency (τ_f) was measured for all the samples and the best value obtained was 9.62 ppm/°C for the sample $MgTiO_3$ added with 12% $CaCu_3Ti_4O_{12}$. The material duly proposed, shows to be promising for applications as dielectric antennas and this study point out that it is possible to obtain a dielectric resonator antenna (DRA) with a temperature coefficient of resonant frequency close to zero.**

Index Terms — $MgTiO_3$, $CaCu_3Ti_4O_{12}$, ceramic, composite, antennas, microwave properties.

I. INTRODUCTION

The Magnesium titanate ($MgTiO_3$) ceramics, commonly called the MTO, is a popular dielectric material applied in microwave frequencies. The MTO has the ilmenite type structure and applications in a microwave frequency range, it exhibits a good quality factor, a low dielectric constant and a temperature coefficient of resonant frequency $\tau_f \sim -50$ ppm/◦C [1]. The MTO is an attractive resonator among microwave materials due to its promising dielectric properties, with moderately high values in quality factors, due to the low cost of raw materials. The MTO compound can also be used as an

Brazilian Microwave and Optoelectronics Society-SBMO received 22 Sept 2016; for review 22 Sept 2016; accepted 11 Feb 2017
Brazilian Society of Electromagnetism-SBMag *© 2017 SBMO/SBMag* *ISSN 2179-1074*

DOI: http://dx.doi.org/10.1590/2179-10742017v16i2794

excellent electrical material employed in microwave components for the usage in radars, GPS and filters [5-6].

The main objective of the present study is to form a composite ceramic to optimize the performance of this particular material, thus, introducing a second phase with a high dielectric constant ($>10^5$), over a wide range of frequency, from -50 ºC to 300 ºC [2-3]. The $CaCu_3Ti_4O_{12}$, ceramics commonly called CCTO, is the subject of many studies in the literature associated with the synthesis and characterization of this said cubic perovskite, due to their unusual electrical properties. The CCTO ceramics is a promising material considering the subject of devices miniaturization to be used by the electronics industry. Oxides with the perovskite structure are well stabilized by their high ε_r values, which allow this particular class of materials to be used in a large number of technological applications. The CCTO can also be used as a sensor for humidity, concentration of O_2 and other applications [4]. The CCTO is considered a good candidate due to its high dielectric constant and a temperature coefficient of resonant frequency τ_f positive. Therefore, the composite MTO-CCTO has thermal stability due near zero temperature coefficient of resonant frequency.

It is important to investigate the electrical behavior of the composite MTO-CCTO in the microwave (MW) range for their possible application as resonator antennas. On the flip side, as a general rule, the demands in the wireless mobile communications, has led to the development of antennas that are low in profile and small in size. Dielectric resonator antennas (DRAs) have been extensively investigated as suitable antennas for wireless applications [7-8]. The DRAs offer attractive features such as low ohmic loss, low profile, small size and relatively wide impedance bandwidth. The DRAs can be used in millimeter frequency bands and being compatible with the existing excitation methods, such as the coaxial probe, microstrip transmission line, co-planar waveguide feed or the aperture coupling. The DRAs are available in basic shapes such as rectangular, cylindrical, spherical and hemispherical geometries.

The DRAs are miniaturized antennas of ceramics. They are fabricated entirely from low loss dielectric materials and being typically assembled on the ground planes. Their radiation characteristics are a function of the mode of operation excited in the DRA. This stated mode is generally chosen based upon the operational requirements. The resonators offer several advantages over other antennas, such as being of a small size with high radiation efficiency and being of simplified coupling schemes for various transmission lines. The bandwidth can be controlled over a wide range by choosing the dielectric constant and geometric parameters of the resonator [9-11].

The cylindrical DRA offers great design flexibility for both, resonant frequency and the Q-factor, which are depending on the radius and/or the height ratio. Various modes can be excited within the DRA and a significant amount of literature is devoted to their field configurations, resonant frequencies and radiation properties [12-13].

 © 2017 SBMO/SBMag

DOI: http://dx.doi.org/10.1590/2179-10742017v16i2794

The main properties required for a DRA are high quality factor (Q), high relative dielectric constant (ε_r) and near zero temperature coefficient of resonant frequency (τ_f). An optimal DRA that satisfies these aforementioned three properties simultaneously is difficult to be achieved in a particular material [15]. Many efforts have been made to control the value of τ_f in the dielectric materials empirically in order to form solid solutions and homogeneous phases mixed with two or more combinations, which are values in the negative and the positive, in order to obtain a coefficient close to zero [16-17], which is required for commercial microwave applications. The mechanisms of the dielectric constant and the dielectric loss variations have been widely investigated.

In this particular investigation, we report the study of the dielectric constant and the dielectric loss of resonators, based on the $MgTiO_3$ ceramic matrix added with the $CaCu_3Ti_4O_{12}$, and the temperature coefficient of resonant frequency (τ_f) in this composite. The experimental and theoretical characteristics of the resonator were properly investigated. The experimental results of the DRA, as introduced by Long and McAllister [7-8], and details of the numerical simulation using the Ansoft HFSS® are given and discussed herein.

II. Experimental Procedure

A. Sample Preparation

The $MgTiO_3$ (MTO) and the $CaCu_3Ti_4O_{12}$ (CCTO) samples were prepared through the solid-state reaction method, in exact accordance with the recent fabrication procedure [17]. The MTO sintered at 1200 ºC has higher porosity, as well as the dielectric constant below standard literature which show that the MTO was sintered at 1350 ºC [18]

Reagents and oxides were accurately weighed in stoichiometric amounts of the $CaCO_3$ (Vetec, 99.0%), CuO (Vetec, 99.0%), TiO_2 (Vetec, 99.0%) and the MgO (Vetec, 99.0%). Previous to the first heat treatment in the high-energy ball milling of the homogeneous powder mixture being conducted in a planetary ball mill for 6 h CCTO and 4h MTO, the rotation speed of the disks carrying the sealed vials was at 360 rpm. The compositions were then calcinated in conventional controlled furnaces at 1000 ºC (CCTO) for 6h and 1100 ºC (MTO) for 4 h, starting from room temperature with a speed of 5 ºC/min. After calcination, the CCTO (4, 6, 8, 10 and 12 wt%) was added to the MTO samples, resulting in five different samples named MCC4, MCC6, MCC8, MCC10 and MCC12. The samples was pressed uniaxially (150 MPa) in a steel die, with a diameter of about 10 mm and a thickness of about 2 mm, hence, transforming the mixture into pellets. These pellets were sintered at 1200 ºC for 5 h in air.

B. X-ray diffraction

The X-ray powder diffraction (XRPD) profiles of the samples were obtained at room temperature (about 294 K), using a powder X-ray diffractometer system Rigaku D/max-B, composed of a X-ray

received 22 Sept 2016; for review 22 Sept 2016; accepted 11 Feb 2017
© 2017 SBMO/SBMag
ISSN 2179-1074

DOI: http://dx.doi.org/10.1590/2179-10742017v16i2794

generator, X-ray optics, goniometer, X-ray detector and counting system, and recorder for data recording or storing. The powder samples were fixed on a silicon plate with a silicon paste. Patterns were collected using CuKα radiation, (λ = 0.15418 nm), operated at 40 kV and 25 mA in the geometry of Bragg-Brentano, with a *0.02º* (*2* step size and a *2*s count time, along angular range *20º - 80º* (*2θ*)). The Rietveld´s method is successfully applied for determination of the quantitative phase abundances in the sintered specimen [19-20].

C. Microwave dielectric properties

The microwave dielectric properties were obtained using the Hakki and Coleman's dielectric resonant TE_{011} and $TE_{01\delta}$ methods [21]. The dielectric loss and dielectric constant were performed in the frequency range of about 8.9–10.5 GHz using network analyzer Agilent N5230A. The values duly obtained in this experiment were used as guides in the numerical simulation of the antennas. The temperature coefficients of resonant frequencies (τ_f) were measured in the temperature range of 22–80 ºC using a new method of measurement described in [22]. The τ_f coefficient was calculated by the following formula:

$$\tau_f = \frac{1}{f_0}\frac{\Delta f}{\Delta T} x10^6 \text{ (ppm/ºC)}, \quad (1)$$

as Δf being the difference between the final and the initial frequencies, ΔT being the difference between the final and initial temperatures and f_0 is the resonance frequency in the beginning of the process.

D. Resonator configuration

The measurements were performed in the transmission/reflection network analyzer, being Agilent N5230A. The DRAs are excited by a wire antenna above a ground plane. The scheme of the cylindrical DRAs is shown in Fig. 1. The DRA is placed above a conducting ground plane (the ground plane is made of copper, 355 mm x 300 mm x 2.14 mm), and excited by a coaxial probe. The coaxial probe went through the ground plane and was connected to an SMA connector. In Fig. 1, the cylindrical DRA has radius a, height h and dielectric constant ε_r of material. The probe was located on the x-axis at x = a and $\phi = 0$.

$$f_0 = \frac{2.997}{2\pi\sqrt{\varepsilon_r}}\sqrt{\left(\frac{1.841}{a}\right)^2 + \left(\frac{\pi}{2h}\right)^2}, \quad (2)$$

 © 2017 SBMO/SBMag *ISSN 2179-1074*

DOI: http://dx.doi.org/10.1590/2179-10742017v16i2794

Eq. (2) was obtained based upon the hypothesis that the lateral and the upper surfaces of the DRA being magnetic conductors perfectly. Since this assumption is verified only for the infinite dielectric constant, Eq. (2) is only an approximation that leads to an error around 10%.

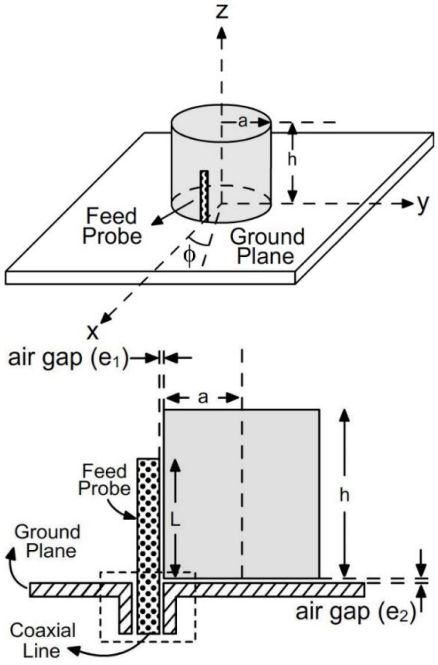

Figure 1: The geometry of the cylindrical resonator antenna.

It would be interesting to compare the values issued from Eq. (2) to the following closed form expression for the $HEM_{11\delta}$ resonant frequency:

$$f = \frac{6.324c}{2\pi a\sqrt{\varepsilon_r + 2}}\left(0.27 + 0.36\frac{a}{2L} + 0.02\left(\frac{a}{2L}\right)^2\right) \tag{3}$$

Using a curve fitting procedure on the numerical experiments based on the method of moments, the Eq. (3) has duly been proposed by Kishk *et al*. [23] for ε_r = 38, and has also been generalized by Mongia and Bhartia [24]. It is important to note that both experimental and simulation results showed great variability in the results, according to the DRA distance to the probe. This particular challenge finds its origin in the presence of an air gap between the dielectric resonator and the metallic conductors, which have been thoroughly studied previously [26]. Furthermore, in order to illustrate the relevant effect, we defined in Fig. 1 two parameters associated with the air gap e_1 between the dielectric and the probe, and e_2 between the dielectric and the ground plane.

E. S parameter

As a result of the high resonant structure of the DRA, the input impedance Z = R + jX at the feeder port presents a frequency response due to the resonant response of each mode. Neglecting the overlap

 © 2017 SBMO/SBMag *ISSN 2179-1074*

DOI: http://dx.doi.org/10.1590/2179-10742017v16i2794

between the first and the second modes, at the resonant frequency of the f_0, the resistance R would show a maximum and the reactance X is null. This said behavior is illustrated in Fig. 5 for the Return Loss (S_{11}). It must be stressed that the derivation of resonant frequencies from the minimum of the return loss parameter S_{11} is not direct, as shown herein. The return loss S_{11} is related to Z by:

$$S_{11} = \frac{z-1}{z+1}; \text{ with } z = \frac{Z}{R_C} \tag{4}$$

as R_c is the characteristic impedance of the feeder. The Eq. (4) shows clearly that S_{11} depends on the R_c: using an R_c = 50 Ω feeder, it will be noted that the power transmission to the antenna is high ($S_{11} \neq 0$) in the resonant frequency of the DRA.

F. Numerical simulation

Another objective of this study is a numerical validation of the experimental set up, following the study of Kiang [27]. As a first advantage, one can investigate the influence of the probe in the resonant frequencies, once Eqs. (2) and (3) concern solely the DRAs without any probe. Secondly, the high sensitivity of the results as a function of the air gap confirms the HFSS® software providing the radiation pattern of these antennas.

An adaptive configuration of discretization was used and convergence is completed for a frequency variation that was inferior to 1%. An eigensolver was employed, in which the resonant frequencies of the structure presented in Fig. 1 were determined by an unexcited feeder along the boundaries of volume of air promoting the impedance matching through small adjustments. An analysis of the first mode in cartography showed that the field pattern inside the DRA was similar to the $HEM_{11\delta}$ mode of the probeless configuration. However, one can notice the existence of a strong field in the probe vicinity, particularly on the interface with the DRA. This fact explains the high sensitivity of the DRA location, as well as discretization errors of the finite-element method.

Instead of the previous eigenmode analysis, the results presented in this study were issued from a harmonic analysis, where the feeder is excited. This stated method enables the determination of the port characteristics, such as the input impedance and the return loss. In order to take into account the effect of an air gap between the probe and the DRA, the gaps e_1 and e_2 (see Fig. 1) were estimated and presented as one of the input parameters for the numerical simulation.

III. RESULT AND DISCUSSION

A. Structural analysis

The formation of the two following phases, CCTO and MTO, was confirmed by X-ray diffraction (XRD) at room temperature in the composite ceramic. In addition, the XRD patterns of the samples in Fig. 2 indicated that both of the sintered CCTO and MTO ceramic were single phase. This fact was

received 22 Sept 2016; for review 22 Sept 2016; accepted 11 Feb 2017
© 2017 SBMO/SBMag
ISSN 2179-1074

DOI: http://dx.doi.org/10.1590/2179-10742017v16i2794

obtained using the program DBWS9807a [28, 29] in Rietveld analysis of the X-ray powder diffraction patterns. Two main phases were observed and identified with the MTO-CCTO (see Fig. 3). The diffraction peaks presented by all samples were identified by the ICSD/95714 (CCTO) and the ICSD/55285 (MTO). Table 1 shows the refinement parameters *S* and R_{wp}, as well as the net parameters (a, b and c) for the DRX analysis through the Rietveld method of refinement for the samples.

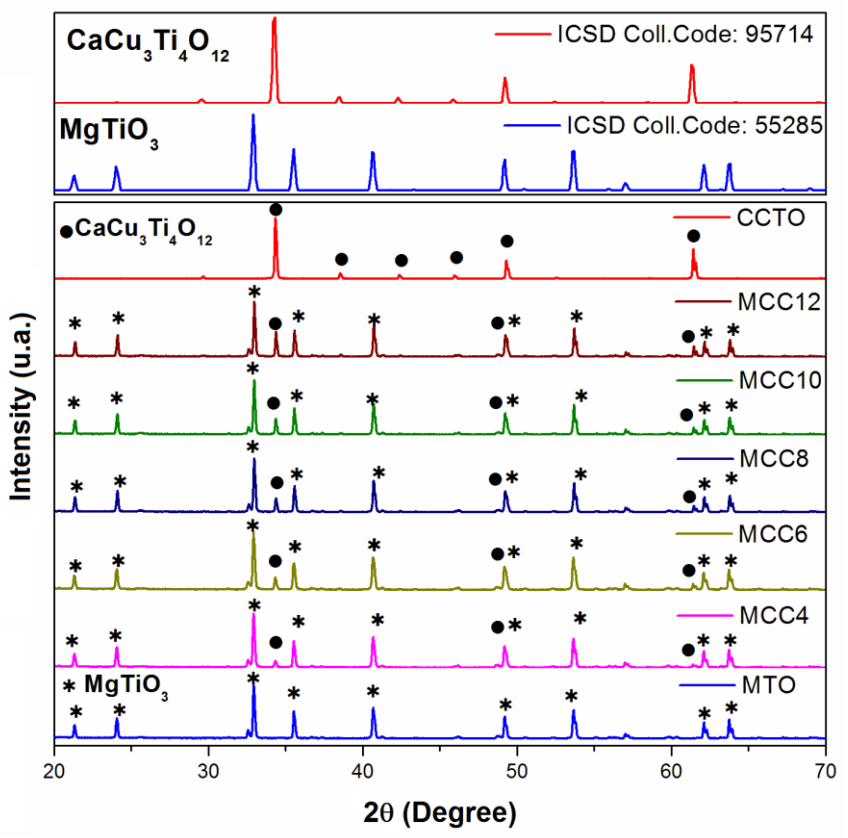

Figure 2: single phase obtained with program DBWS9807a for Rietveld analysis of X-ray powder diffraction patterns of (a) CCTO (b) MCC12 and (b) MTO ceramics sintered at 1200 ºC in air for 5 h: Y_{obs} indicates the data of experiments. Y_{calc} shows the data of calculation. Dif. shows the diference (Y_{obs} - Y_{calc}).

Table 1: Rietveld Analysis for the samples of MTO-CCTO and MCC12 obtained from X-ray.

Refinement parameter	Samples			
	MTO	CCTO	MCC12	
R-WP	22.47	8.52	17.52	
S	1.63	1.01	1.44	
			MTO	CCTO
R_{Bragg}	5.29	3.29	8.76	8.44
%	100	100	89.20	10.80
Density (g/cm^3)	3.895	5.055	3.895	5.055
a	5.055	7.391	5.055	7.391
b	5.055	7.391	5.055	7.391
c	13.899	7.391	13.899	7.391

© 2017 SBMO/SBMag

DOI: http://dx.doi.org/10.1590/2179-10742017v16i2794

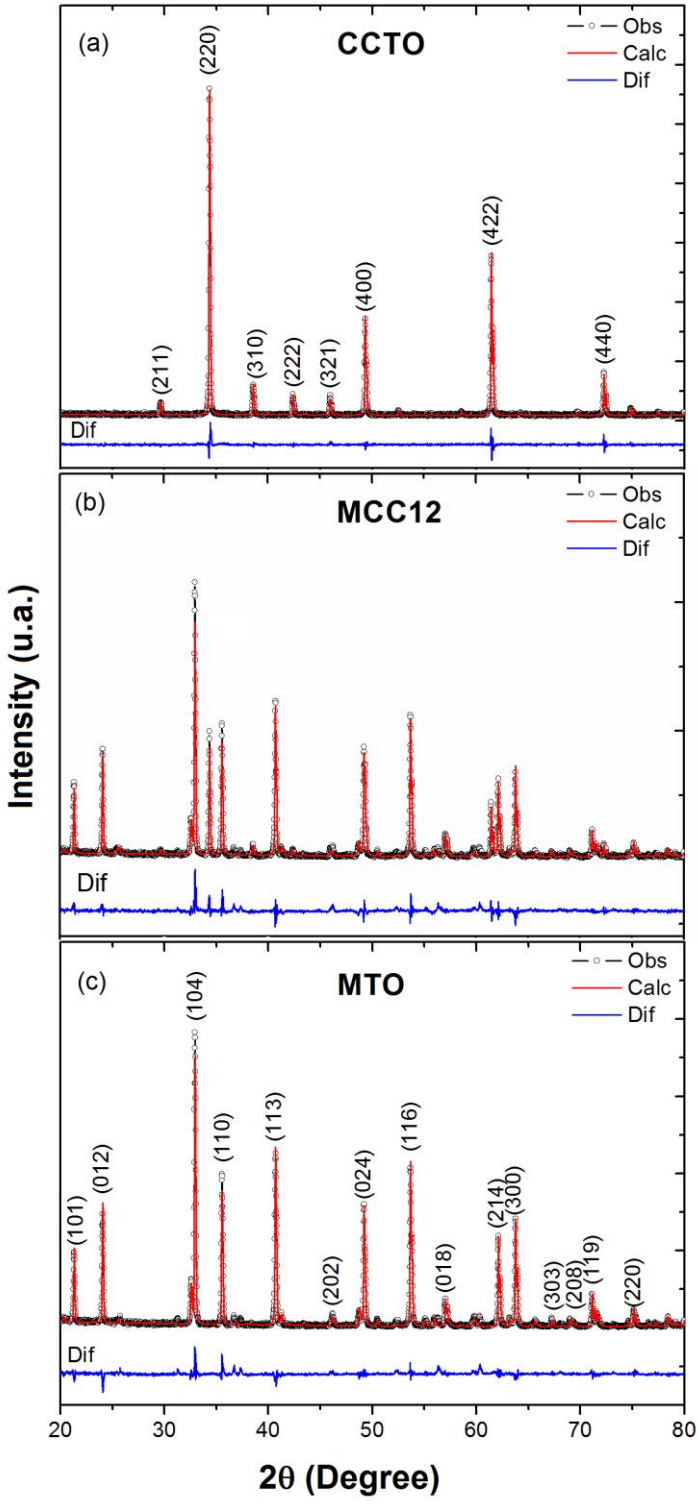

Figure 3: X-ray diffraction patterns of MTO-CCTO samples, sintered at 1200 ºC/5 h

Fig. 4 showed the scanning electron microscopy (SEM) and the micrographs reveal that the increasing addition of the CCTO promotes grain growth and reduction of the porosity. The pure MTO showed high porosity due to the temperature sintering using unconventional.

 © 2017 SBMO/SBMag *ISSN 2179-1074*

DOI: http://dx.doi.org/10.1590/2179-10742017v16i2794

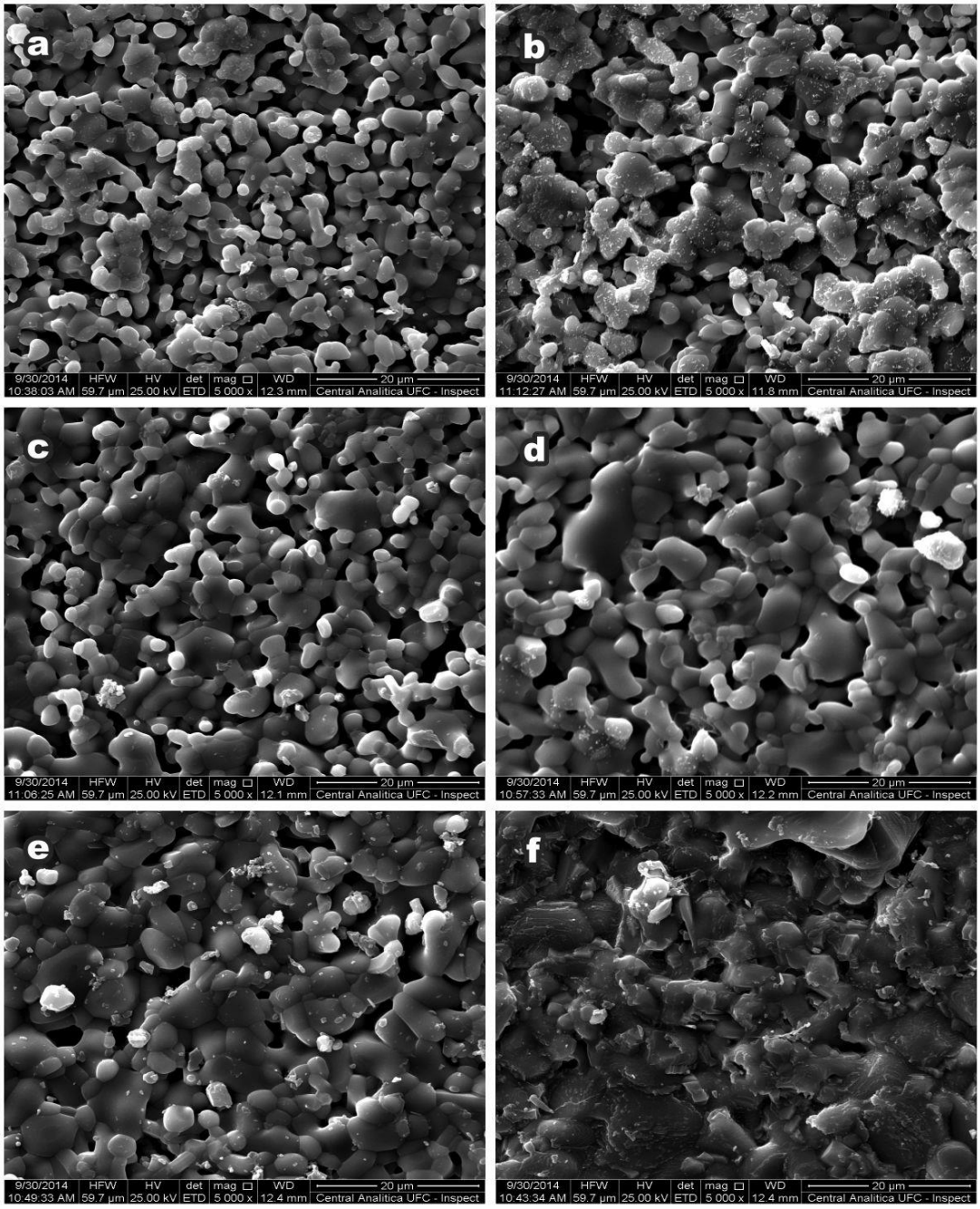

Figure 4: Microstructure of the sintered ceramics (a) MTO, (b) MCC4, (c) MCC6, (d) MCC8, (e) MCC10 and (f) MCC12.

B. Microwave dielectric properties

The dielectric loss (tg δ) and the dielectric constant (ε_r) duly obtained from the resonant frequency of the TE_{011} mode in the Hakki and Coleman´s method are shown on Table 2. The dielectric constant increased with the increasing addition of the CCTO and this is due to the decreased porosity and the increased density, as well as the dielectric constant high of the CCTO (see Table 2). The dielectric loss decreases for the samples MCC4 and MCC6, when compared with the MTO. This is due to the increased grain and the small addition of the CCTO, which promotes a better filling in the pores.

 © 2017 SBMO/SBMag

DOI: http://dx.doi.org/10.1590/2179-10742017v16i2794

Concerning the MCC8, MCC10 and MCC12, the dielectric constant increase suggested greater influence to the CCTO than to the composite.

Table 2: Microwave measurements of the samples obtained through the Hakki–Coleman (Courtney) method.

Samples	ε_r	τ_F *(ppm/°C)**	$tg\delta\,(10^{-4})$	f_0 *(GHz)*	ρ *(g/cm^3)*	e_1 *(μm)*	e_2 *(μm)*	*a (mm)*	*h (mm)*
MTO	11.54	-39.25	6.71	10.52	2.63	85	70	6.00	5.70
MCC4	14.03	-39.00	4.82	9.75	3.08	86	68	5.85	5.60
MCC6	16.33	-38.84	3.52	9.52	3.37	49	11	5.67	5.25
MCC8	18.86	-30.85	5.70	8.94	3.50	54	26	5.55	5.25
MCC10	20.44	-12.73	7.05	8.94	3.67	60	13	5.50	4.95
MCC12	21.01	9.62	8.62	8.89	3.74	75	12	5.47	4.90

All the stated samples showed resonant frequency (f_0) between 8.892 GHz and 10.527 GHz. The highest dielectric constant was obtained for the MCC12 sample (ε_r = 21.01) due to a higher densification.

C. Studies of the $MgTiO_3 – CaCu_3Ti_4O_{12}$ resonator antenna

Regarding the application in dielectric resonator antennas, it is necessary to have a combination with the dielectric constant, dielectric losses and temperature coefficient of the resonant frequency (τ_f). The temperature coefficient of resonant frequency (τ_f) for all samples is shown on Table 2. The τ_f indicates how much the resonant frequency drifts with the changing temperature denoting the thermal stability of the material [14]. The sample MCC12 had the best value of the thermal stability (9.62 ppm/ºC) and presented good result for microwave applications, since τ_f values were lower than 10 ppm/ºC, being necessary for these applications [14].

The frequency response around the first mode ($HEM_{11\delta}$) was determined by the HFSS® and the result is compared to one of the experiment. Hence, results properly obtained were reported for the input impedances, return loss, radiation patterns and the Smith Charts.

However, different resonant modes have distinct electromagnetic field distributions within the DRA and each mode may provide a different radiation pattern [22]. The mode with the lowest resonant frequency is the fundamental broadside $HEM_{11\delta}$.

The considerations herein related to the air gap between the probe, the resonator, and the ground plane carried out in this study, were essential to the improvement of the results through the numerical procedure. The values used in the simulation to the air gap (e_1 and e_2), influence the impedance matching between the dielectric resonator and the transmission line. The adjustment of the magnitude in the return loss was also influenced by air gaps. Another critical parameter for the best fit of the experimental curve simulated, was adjusting the permittivity and the dielectric loss. The permittivity adjusted the positioning of the return loss curve in the frequency range and a dielectric loss have

 © 2017 SBMO/SBMag *ISSN 2179-1074*

DOI: http://dx.doi.org/10.1590/2179-10742017v16i2794

influence in the setting of bandwidth. On Table 3 and in Fig. 5, the theoretical and experimental results for the return loss (S_{11}) of cylindrical antennas are shown, respectively.

Accordance between the experimental and the numerical results in the return loss do have good agreement (Fig. 5) and the error in the measured/simulated frequency is less than 0.1% for all samples. As for the value of the S_{11} the error is higher for MCC6 (13.67%) while the other samples presented the error between 0.4% and 2.5% (see Table 3).

Table 3: Theoretical/experimental frequencies and air-gaps assigned for numerical procedures of cylindrical antennas

	Samples	**MTO**	**MCC4**	**MCC6**	**MCC8**	**MCC10**	**MCC12**
ε_r		11.54	14.03	16.33	18.46	20.44	21.01
$f_{HEM11\delta}$ (GHz)	SIM	6.109	5.798	5.692	5.556	5.474	5.524
	EXP	6.107	5.798	5.697	5.554	5.475	5.523
	E_r (%)	0.03	0	0.09	0.03	0.02	0.02
S_{11} (dB)	SIM	- 35.12	- 27.52	- 41.76	- 37.11	- 26.96	- 29.85
	EXP	- 35.91	- 28.20	- 47.47	- 36.71	- 26.79	- 29.15
	E_r (%)	2.25	2.47	13.67	1.08	0.63	2.34
Peak resonant resistance (Ω)	SIM	168.63	144.14	161.16	148.18	128.30	131.67
	EXP	236.76	194.19	208.30	176.85	202.34	160.88
	E_r (%)	40.40	34.72	29.25	19.34	57.71	22.18
Resistance (Ω) $f_{HEM11\delta}$	SIM	48.28	53.65	50.05	49.03	52.25	51.92
	EXP	48.42	53.14	49.72	51.23	46.35	52.11
	E_r (%)	0.29	0.95	0.66	4.49	11.29	0.36
BW (%)	SIM	10.7	7.9	6.7	6.2	5.1	5.9
	EXP	9.1	6.6	6.1	5.3	5.0	5.2
	E_r (%)	14.95	16.45	8.95	14.51	1.96	13.46
Gain (dB)		2.75	3.47	3.62	3.88	3.92	4.03
e_{CD} (%)		98.71	98.78	98.80	98.84	98.89	98.90

Such a behavior has been explained in literature [25; 26]. The resistance R of the first resonant frequency of each antenna was also indicated on Table 3 and in Fig. 8. The best compromise between the experimental and simulated resistance occurred in the sample MCC8 (19.34%).

In order to get a more precise behavior, the complex S_{11} was reported in the Smith Chart for the MCC12 in Fig. 7. Regarding the other five dielectric samples, the Smith Chart was quite similar. Usually, it was noticed that a good agreement was obtained between the simulation with the HFSS® modeling and the experimental methodology, which verified the effectiveness of DRAs modeling using the Ansoft's HFSS®.

 © 2017 SBMO/SBMag

DOI: http://dx.doi.org/10.1590/2179-10742017v16i2794

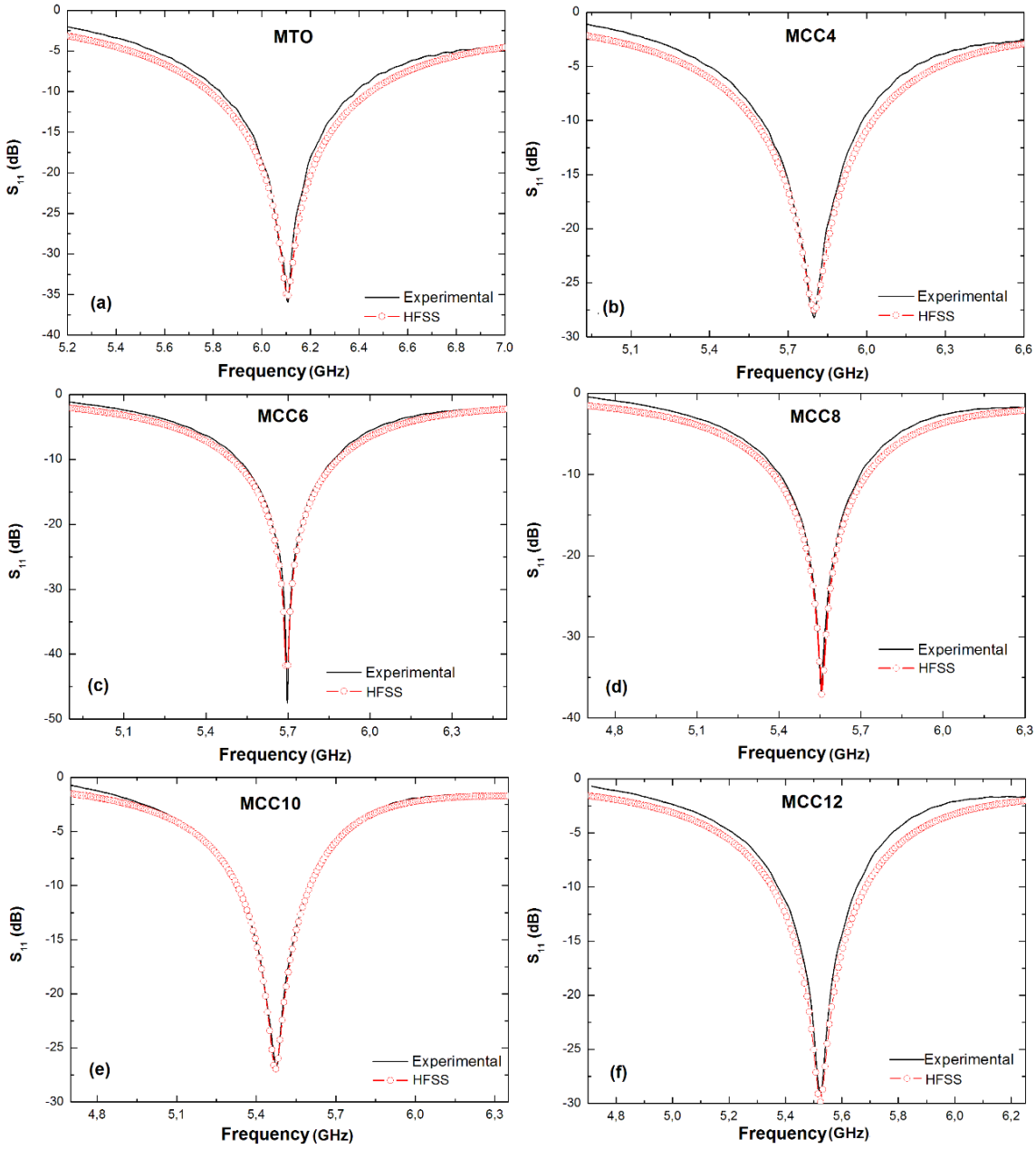

Figure 5: Experimental and theoretical HFSS Return loss (S11) of cylindrical resonators (a) MTO, (b) MCC4, (c) MCC6, (d) MCC8, (e) MCC10 and (f) MCC12.

The agreement between the experimental and the theoretical value is good. However, one can notice as well that the minimum of $|S_{11}|$ was not situated in the null reactance curve of the Smith Chart (Fig. 7). Therefore, Z is not real at f_0, as the graphic of Z, given in Fig. 6. For this stated reason, the minimum of $|S_{11}|$ does not coincide exactly with the zero of the imaginary part of Z.

© 2017 SBMO/SBMag

DOI: http://dx.doi.org/10.1590/2179-10742017v16i2794

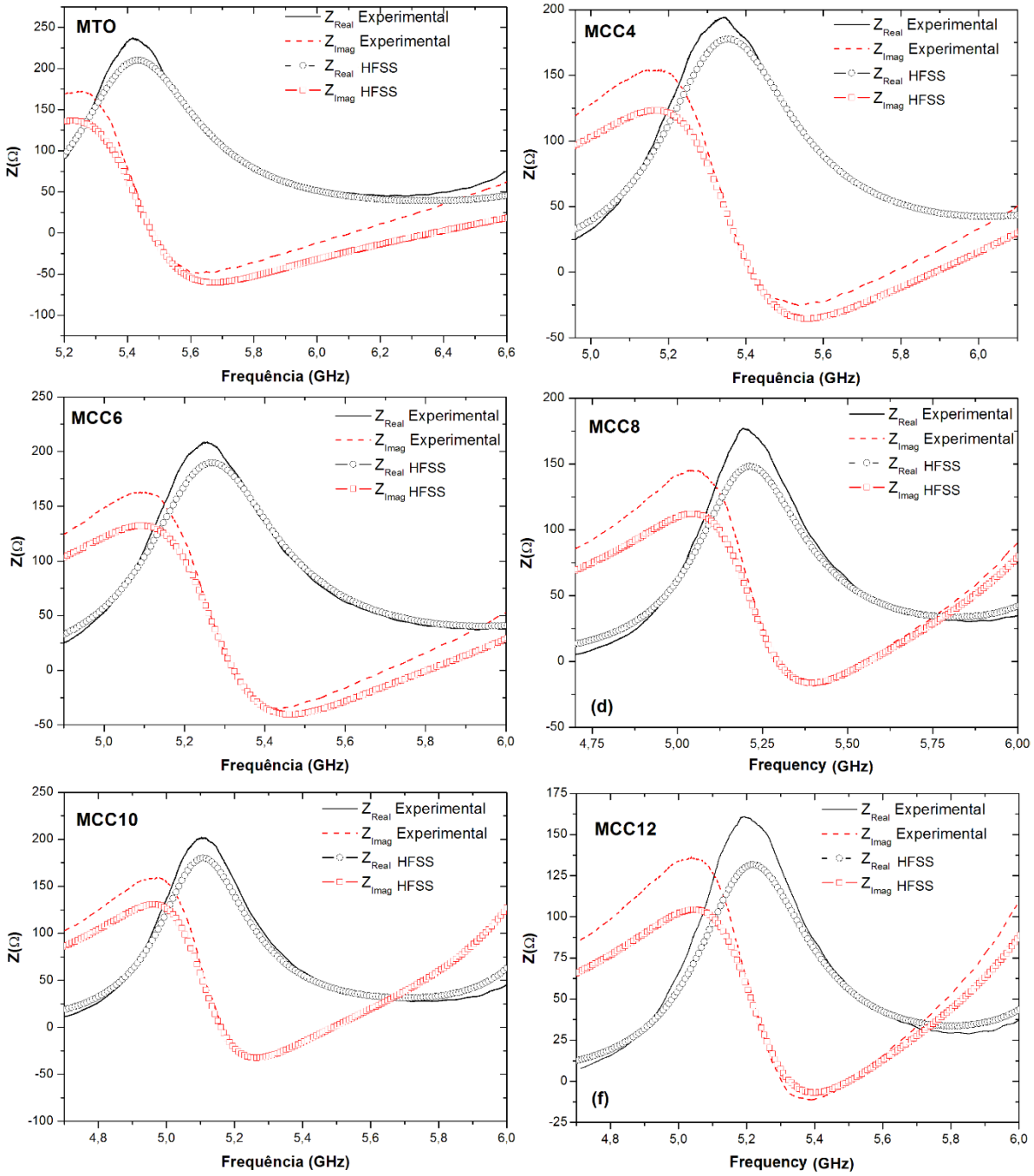

Figure 6 Experimental and theoretical HFSS input impedance (Z) of cylindrical resonators (a) MTO, (b) MCC4, (c) MCC6, (d) MCC8, (e) MCC10 and (f) MCC12.

The aforesaid calculated radiation pattern of the E_θ plane and the E_φ plane in the resonant frequency of the MTO samples, are shown in Fig. 8. Regarding the other five dielectric samples, the radiation pattern was quite similar. The symmetries of the field patterns were related to the feed probe location at ($\theta = 0^o$) and the duly obtained values for the x–z plane (Fig. 8) showed a broad and almost an omnidirectional pattern with a roll-off near $\theta = 90^o$ (a consequence of the finite ground plane used for the experimental set up). These stated results are in agreement with data reported in the literature [10].

 © 2017 SBMO/SBMag *ISSN 2179-1074*

DOI: http://dx.doi.org/10.1590/2179-10742017v16i2794

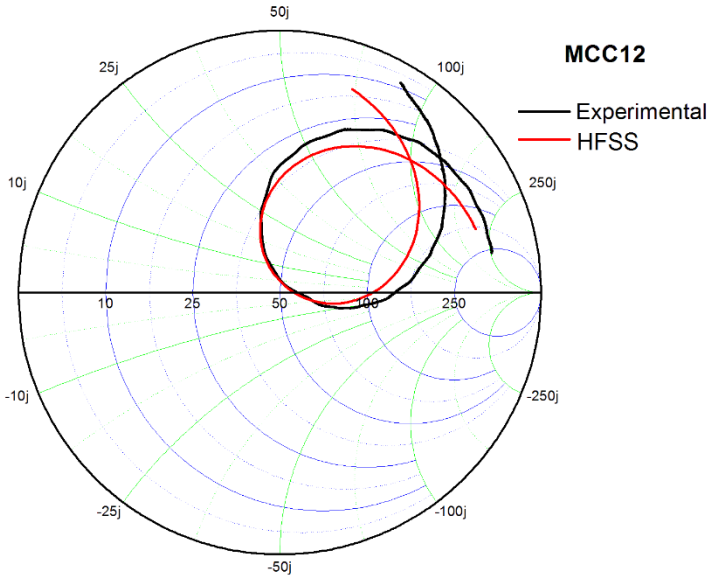

Figure 7: Experimental and theoretical HFSS input impedance Smith Chart of cylindrical resonators of MCC12.

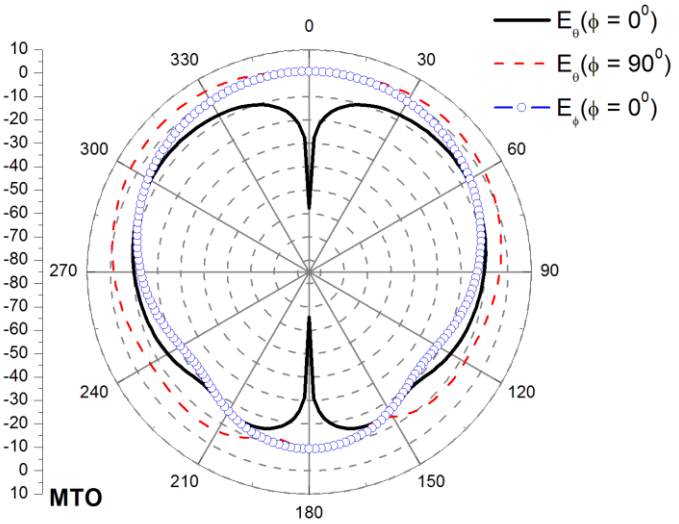

Figure 8: Simulated radiation pattern of E_θ ($\varphi = 0^o$), E_θ ($\varphi = 90^o$) and E_φ ($\theta = 0^o$) of MTO.

The gain of an antenna is defined as "the ratio of intensity in a given direction in relation to the radiation intensity that was duly properly obtained, if the power accepted by the antenna was radiated isotropically" [30; 31]. With a little amount of the CCTO doped into the MTO, there was a gain increase from the 2,75 dB (pure MTO) to the 4,03 dB (MCC12) (see Table 3).

IV. CONCLUSIONS

This study describes an experimental and numerical investigation of the dielectric properties in microwave of the ceramic resonators matrix, based on the $MgTiO_3$. The materials were obtained from a route in the solid-state procedure. The dielectric resonator antenna (DRA) has been investigated taking advantage in the configuration of a monopole thorough an infinite ground plane and using the

 © 2017 SBMO/SBMag

DOI: http://dx.doi.org/10.1590/2179-10742017v16i2794

Ansoft's HFSS®. An Excellent agreement between the simulation and the experimental results, was duly obtained. The $MgTiO_3$ ceramic matrix presents a dielectric constant between 11.54 and 21.01. The antenna bandwidth was in the range of 5.0 and 9.1%. The temperature coefficient of resonant frequency (τ_f) from the MTO showed values in the range of -39.25 ppm $^oC^{-1}$ to 9.62 ppm $^oC^{-1}$. The sample of the MCC12 has value of the thermal stability of 9.62 ppm/^{o}C and permissivity of 21.01 as well as dielectric loss of 8.62 x 10^{-4}. The result is in good agreement for the microwave applications. In summary, the performance in the microwave region of the dielectric ceramic cylindrical samples based in the $MgTiO_3$, confirms the potential use of such said materials for the small DRAs.

V. ACKNOWLEDGMENTS

The authors thank the LOCEM (Laboratory of Telecommunications and Materials Science and Engineering), the Departments of Physics and Teleprocessing, the x-ray laboratory of the Federal University of Ceará, Brazil, and Central Analytical Department of the Federal University of Ceará.

REFERENCES

[1] C. L. Huang, C. H. Shen, C. L. Pan, Materials Science and Engineering B 145, *Elsevier*, pp. 91–96, 2007.
[2] P. Lunkenheimer, V. Bobnar, A. V. Pronin, A. I. Ritus, A. A. Volkov, and A. Loidl, *Phys. Rev. B*, vol. 66, no. 052105, 2002.
[3] M. H. Cohen, J. B. Neaton, L. X. He, and D. Vanderbilt, *J. Appl. Phys.*, vol. 94, no. 5, pp. 3299–306, 2003.
[4] M. Li, X. L. Chen, D. F. Zhang, W. Y. Wang, and W. J. Wang, *Sens. Actuators B-Chem.*, vol. 147, no. 2, pp. 447–52, 2010.
[5] J. Y. Chen and C. L. Huang, *Mater. Lett.*, vol. 64, no. 23, pp. 2585–8, 2010.
[6] H. Jantunen, R. Rautioaho, A. Uusimaki, and S. Leppavuori, *J. Eur. Ceram. Soc.*, vol. 20, no. 14–15, pp. 2331–6, 2000.
[7] M.W. McAllister, S.A. Long, G.L. Conway, *IEEE Electron. Lett.*, vol. 19, no. 6, pp. 218–219, 1983.
[8] S.A. Long, M.W. McAllister, L.C. Shen, "The resonant cylindrical dielectric cavity antenna", *IEEE Trans. Antennas Propag.* AP-31, no. 3, pp. 406–412, 1983.
[9] A. Petosa, A. Ittipiboon, Y. Antar, "Dielectric Resonator Antennas, Research Studies", Press Ltd., Hertfordshire, England, UK, 2003, pp. 177–208.
[10] K.M. Luk, K.W. "Leung, Dielectric Resonator Antennas, Research Studies", Press Ltd., Hertfordshire, England, UK, 2003.
[11] D. Pozar, "Microwave Engineering", John Wiley & Sons, Inc., 1998.
[12] D. Kajfez, A. W. Glisson and J. James, *IEEE Trans. Microwave Theory Tech.*, vol.MTT-32, pp. 1609-1616, 1984.
[13] Y. Kobayashi and S. Tanaka, *IEEE Trans. Microwave Theory and Tech.*, vol. 28, pp. 1077-1085, Oct. 1980.
[14] M.T Sebastian, "Dielectric Materials for Wireless Communication", Elsevier, 2008.
[15] A.D.S.B. Costa, D.G. Sousa, R.C.S. Costa, F.W.de O. Amarante, T.S.M. Fernandes, G.D. Saraiva, M.A.S. da Silva, A.S.B. Sombra, *Phys. Scr*., vol. 84, 2011.
[16] H.O. Rodrigues, A.J.M. Sales, G.F.M. Pires Junior, J.S. Almeida, M.A.S. Silva, A.S.B. Sombra, *J. Alloys Compd*, vol. 576, pp. 324–331, 2013.
[17] H.O. Rodrigues, G.F.M. Pires Junior, J.S. Almeida, E.O. Sancho, A.C. Ferreira, M.A.S. Silva, A.S.B. Sombra, *J. Phys. Chem. Solids*, vol. 71, pp. 1329–1336, 2010.
[18] J. Bernard, F. Belnou, D. Houivet, J. M. Haussonne, "Low sintering temperature of $MgTiO_3$ for type I capacitors"., *Journal of the European Ceramic Society*, vol. 25, pp. 2779–2783, 2005.
[19] H.M. Rietveld, *Acta Crystallography*, vol. 22, pp. 151, 1967.
[20] H.M. Rietveld, *J. Appl. Crystallography*, vol. 2, pp. 65, 1969.
[21] B.W. Hakki, P.D. Coleman, "A dielectric resonator method of measuring inductive capacities in the millimeter range", *IRE Trans. Microw. Theory Tech*. MTT-8, pp. 402–410, 1960.
[22] M.A.S. Silva, T.S.M. Fernandes, A.S.B. Sombra, *J. Appl. Phys.* vol. 112, no. 074106, 2012. [Online]. Available: http://dx.doi.org/10.1063/1.4755799.
[23] A.A. Kishk, A.W. Glisson, D. Kajfez. "Computed Resonant Frequency and Far Fields of Isolated Disks", *IEEE AP-S International Symposium Digest*, vol. 1, pp. 408–411, 1993.
[24] R.K. Mongia, P. Bhartia, *Int. J. Microw. Millimeter-Wave Computer-Aided Eng.*, vol. 4, no.3, pp. 230–247, 1994.
[25] G.P. Junker, A.A. Kishk, A.W. Glisson, D. Kajfez, *IEEE Electron. Lett.*, vol. 30, no. 2, pp. 97–98, 1994.
[26] P. B. a. Fechine, H. H. B. Rocha, R. S. T. Moretzsohn, J. C. Denardin, R. Lavín, and a. S. B. Sombra, *IET Microwaves, Antennas Propag.*, vol. 3, pp. 1191–2009, 2008.

 © 2017 SBMO/SBMag

DOI: http://dx.doi.org/10.1590/2179-10742017v16i2794

[27] J.F. Kiang, "Novel Technologies for Microwave and Millimeter Wave Applications", Kluwer Academic Publishers, Boston, 2004.
[28] Bleicher L, Sasaki JM, Santos COP. "Development of a graphical interface for the Rietveld refinement program DBWS". *J Appl Crystallography*, vol. 33, no. 4, pp. 1189, 2000.
[29] Young RA, Sakthivel A, Moss TS, Paiva-Santos "CO. DBWS-9411–an upgrade of the DBWS*.* programs for Rietveld refinement with PC and mainframe computers". *J Appl Crystallography*, vol. 28, no. 3, pp. 366–367, 1995
[30] Z. Peng, F. Wang, X. Yao, *Ceram. Int*., vol. 30, pp. 1211–1214, 2004.
[31] E. Carvalho, M. Bertolete, I. F. Machado, E. N. S. Muccillo. "Characterization of the perovskite $CaCu_3Ti_4O_{12}$ consolidated by field-assisted sintering", *Cerâmica.*, vol. 59, pp. 293-301, 2013.

received 22 Sept 2016; for review 22 Sept 2016; accepted 11 Feb 2017
© 2017 SBMO/SBMag
ISSN 2179-1074